Eur Biophys J (2016) 45:149–163
DOI 10.1007/s00249-015-1084-z

ORIGINAL ARTICLE

EBSA
Biophysics in Europe

Lipid dynamics in boar sperm studied by advanced fluorescence imaging techniques

Filip Schröter[1] · Ulrike Jakop[1] · Anke Teichmann[2] · Ivan Haralampiev[3] · Astrid Tannert[1] · Burkhard Wiesner[2] · Peter Müller[3] · Karin Müller[1]

Received: 7 July 2015 / Revised: 9 September 2015 / Accepted: 17 September 2015 / Published online: 19 October 2015

Abstract The (re)organization of membrane components is of special importance to prepare mammalian sperm to fertilization. Establishing suitable methods to examine physico-chemical membrane parameters is of high interest. We characterized the behavior of fluorescent (NBD) analogs of sphingomyelin (SM), phosphatidylserine (PS), and cholesterol (Ch) in the acrosomal and postacrosomal macrodomain of boar sperm. Due to their specific transverse membrane distribution, a leaflet-specific investigation of membrane properties is possible. The behavior of lipid analogs in boar sperm was investigated by fluorescence lifetime imaging microscopy (FLIM), fluorescence recovery after photobleaching (FRAP), and fluorescence correlation spectroscopy (FCS). The results were compared with regard to the different temporal and spatial resolution of the methods. For the first time, fluorescence lifetimes of lipid analogs were determined in sperm cell membrane and found to be in a range characteristic for the liquid-disordered phase in artificial lipid membranes. FLIM analyses further indicate a more fluid microenvironment of NBD-Ch and NBD-PS in the postacrosomal compared to the acrosomal region. The concept of a more fluid cytoplasmic leaflet is supported by lower fluorescence lifetime and higher average *D* values (FCS) for NBD-PS in both head compartments. Whereas FLIM analyses did not indicate coexisting distinct liquid-ordered and -disordered domains in any of the head regions, comparisons between FRAP and FCS measurements suggest the incorporation of NBD-SM as well as NBD-PS in postacrosomal subpopulations with different diffusion velocity. The analog-specific results indicate that the lipid analogs used are suitable to report on the various physicochemical properties of different microenvironments.

Keywords Boar sperm · Acrosome · Postacrosome · Fluorescence lifetime imaging microscopy · Fluorescence recovery after photobleaching · Fluorescence correlation spectroscopy

Introduction

Mammalian sperm undergo a multitude of complex processes during their maturation, which finally prepares them to fertilize the oocyte. After formation in the testis and passing through the epididymis, sperm still have an inchoate competence for fertilization. Upon ejaculation, they are decorated with proteins priming them for transit through the female genital tract where they have to adapt to changing environmental conditions. At these final steps of maturation, while becoming prepared for the fertilization event, sperm are not able to express proteins on their own (Mackie et al. 2001). Therefore, all necessary adaptations must occur via incorporation of external components or

Electronic supplementary material The online version of this article (doi:10.1007/s00249-015-1084-z) contains supplementary material, which is available to authorized users.

✉ Filip Schröter
schroeter@izw-berlin.de

✉ Karin Müller
mueller@izw-berlin.de

[1] Department of Reproduction Biology, Leibniz Institute for Zoo and Wildlife Research (IZW), Alfred-Kowalke-Straße 17, 10315 Berlin, Germany

[2] Leibniz Institute for Molecular Pharmacology, Berlin, Germany

[3] Department of Biology, Humboldt-University Berlin, Berlin, Germany

reorganization of existing cellular molecules and structures. As the (re)organization of membrane components of the sperm membrane is of special importance in understanding the processes that are prerequisite to fertilization, the establishment of suitable methods to examine physico-chemical membrane parameters is of high interest.

Although mammalian sperm of different species perform similar functions, the membrane lipid composition is highly heterogenic (Fuchs et al. 2009; Lessig et al. 2004). Therefore, it is a challenge for any measurement to apply probes that mimic ubiquitous membrane components and have a minimal influence on the membrane itself. Studies on sperm have mainly used fluorescently labeled lipids and lipid analogs. Fluorescent phosphatidylcholine (NBD-PC), phosphatidylethanolamine (NBD-PE), and cholesterol (NBD-Ch) as well as artificial lipid reporters like 5-(*N*-octadecanoyl) aminofluorescein (ODAF), 1,1′-didodecyl-3,3,3′3′-tetramethylindocarbocyanine ($DiIC_{12}$) and 1,1′-dihexadecyl-3,3,3′3′-tetramethylindocarbocyanine ($DiIC_{16}$) have been applied to analyze diffusion coefficients in sperm of a variety of species by fluorescence recovery after photobleaching (FRAP). Dependent on the species, diffusion of these probes may differ between sperm regions and change upon sperm maturation in the epididymis, after removal of cholesterol, or after addition of hydroperoxides (for review see, Jones et al. 2007, 2010).

Mammalian sperm are strongly laterally organized cells (Fig. 1). Especially the properties of the acrosomal and postacrosomal region during cell maturation have been characterized. In ejaculated boar sperm, it has been shown by fluorescence recovery after photobleaching (FRAP), fluorescence loss in photobleaching (FLIP), atomic force microscopy (AFM), and single particle fluorescence imaging (SPFI) that a "molecular filter" separates the postacrosomal from the acrosomal macrodomain of the sperm head (James et al. 2004; Jones et al. 2010): whereas $DiIC_{12}$ was freely diffusible between the anterior and posterior head membrane, $DiIC_{16}$ formed aggregates of 0.3–1.0 µm in diameter, which only rarely crossed the equatorial segment. The lateral heterogeneity of plasma membrane components by formation of microdomains and its relevance for physiological processes has been investigated intensively in mammalian cells, and is currently also under investigation for mammalian sperm (Kawano et al. 2011). Diffusion characteristics, and their local variation in response to external stimuli, may play a crucial role in the formation of this lateral membrane structure and can be studied amongst others by FRAP.

Whereas SPFI is mainly restricted to proteins and lipid aggregates, there are further fluorescence methods besides FRAP which allow gathering information on parameters of membrane inherent lipid markers as for example fluorescence correlation spectroscopy (FCS) and fluorescence lifetime imaging microscopy (FLIM). Each of these methods has a different temporal and spatial resolution so that the information gained can be interpreted as snapshot of the conditions over a defined time period and area (see below).

Experiments with FRAP are carried out by irreversibly bleaching the fluorophores in a defined bleaching spot and detecting the recovery rate of fluorescence. Thereby a diffusion coefficient of the fluorophore can be calculated. The size of bleaching spots has a dimension of micrometers in diameter and bleaching times of 5–50 ms are used. Measurements with this technique are usually performed within seconds with the data points most relevant for fitting the recovery curve being collected within the first 2 s.

FCS measures fluorescence fluctuation in a very small volume thus detecting the changes in fluorescence intensity caused by Brownian motion of the fluorophores. These data allow, amongst others, the calculation of diffusion coefficients of the fluorescent molecules. The detected diffusion times in the confocal volume [ω_1 (488 nm) = 230 nm] are in the dimensions of milliseconds.

The measurement of fluorescence lifetime mainly provides information on the immediate vicinity of the examined fluorophore and depends particularly on mobility and polarity of its surroundings. If the fluorophore possesses a dipole moment in the ground state that changes upon excitation, as NBD does, a red shift of the emission spectrum in polar solvents can be detected. This is caused by the reorientation of the surrounding polar solvent molecules to realign the dipole moments. While this reorientation/relaxation process does not significantly affect the fluorescence lifetime in fluid environments, it does when the viscosity of the surroundings is high. Since the speed of the relaxation crucially depends on the movement of the involved molecules, an increased environmental fluidity decreases the fluorescence lifetime by shortening the relaxation process. Along the vertical axis and horizontal plane of a membrane,

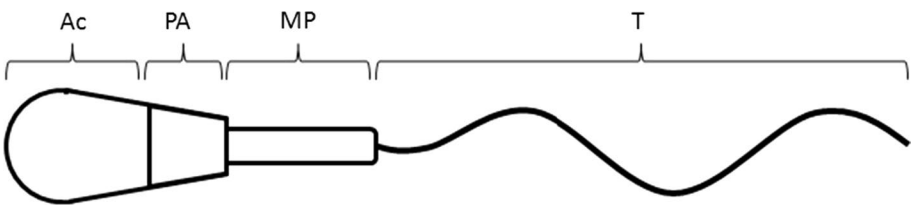

Fig. 1 Schematic view of the lateral organization of mammal spermatozoa. *Ac* acrosomal region, *PA* postacrosomal region, *MP* midpiece, *T* tail

different microenvironments varying in mobility and polarity exist (Amaro et al. 2014; de Almeida et al. 2009).

Since the abundance and distance of possible interaction partners like said polar solvent molecules or quencher molecules also affects the fluorescent lifetime, FLIM enables the investigation of domain formation by tracing interactions between reporter molecules and their surroundings whereas FRAP and FCS mainly address the diffusion properties of reporter molecules.

Fluorescence lifetime measurements reflect the environmental conditions of labels in a very short time frame (nanoseconds). However, it is important to note that the fluorescence lifetimes of all fluorophores in a given membrane area are recorded over a longer period (microseconds per pixel). Only if substantial structural inhomogeneities lead to explicit lifetime differences for embedded label molecules and are stable over a time period of about three times their fluorescence lifetime, they might be detected down to a size of about 10 nm^2 (Stöckl et al. 2008).

Here, we have characterized the behavior of fluorescent (NBD) analogs of SM, PS, and Ch in the acrosomal and postacrosomal macrodomain of boar sperm. Although these analogs have a short fatty acyl chain and an artificial NBD moiety, they have been successfully employed to investigate the role of lipids for various biological processes, such as transbilayer movement of lipids, lipid–protein interactions, lipid–bile salt interactions, and intracellular transport processes of lipids (Eckford and Sharom 2005; Im et al. 2004; Kol et al. 2003; Pomorski et al. 1994; Tannert et al. 2007a; Wustner et al. 2001, 1998). It has been shown that these analogs—albeit with certain limitations (Haldar and Chattopadhyay 2013; Wustner 2007)—reflect properties of the respective endogenous lipids. For example, they have been used for characterizing the transbilayer distribution and mobility in plasma membranes of numerous cells. Those measurements have shown that NBD-SM is exclusively localized in the outer membrane leaflet. In contrast, NBD-PS is rapidly transported to the inner membrane leaflet accumulating in this layer (Zachowski 1993). This behavior of NBD-SM and NBD-PS has also been shown in the plasma membrane of sperm cells including those of the boar (Gadella et al. 1999; Kurz et al. 2005; Müller et al. 1994; Nolan et al. 1995). Notably, these transbilayer characteristics of phospholipid species has been found by other approaches also using differently labeled analogs (Daleke 2003; Pomorski et al. 2001; Zachowski 1993). For NBD-Ch, a very rapid, protein-independent transbilayer movement and a symmetrical transverse distribution can be assumed (Müller et al. 2011). Moreover, NBD-labeled lipid analogs have also been successfully applied especially for FLIM (Klein et al. 2012; Ostasov et al. 2013; Stöckl et al. 2008) and FRAP analysis (Christova et al. 2004; Pucadyil et al. 2007).

Membrane fluidity and domain formation in the acrosomal and postacrosomal part of the mammalian sperm cell membrane are key elements for membrane stabilization before and creation of fusion competence after capacitation. Therefore, the behavior of the NBD-labeled lipid analogs in boar sperm was investigated by performing FLIM, FRAP, and FCS measurements. An advantage of using these reporter molecules is that due to their specific transverse distribution in the membrane, a leaflet-specific investigation of membrane properties is possible. The results obtained by the various methods were critically compared with regard to their different temporal and spatial resolution reflecting different organizational membrane structures or properties in vital cells. The outcome of the presented approaches in ejaculated sperm is prerequisite to their further application examining the diverse sperm membrane interactions with molecules in seminal fluid, female genital tract as well as changes during capacitation and further stages of the fertilization process.

Materials and methods

Materials

All chemicals and solvents were obtained in the highest commercially available purity. NBD-labeled lipids were purchased from Avanti Polar Lipids (Birmingham, AL, USA): *N*-[6-[(7-nitro-2-1,3-benzoxadiazol-4-yl) amino]caproyl]-sphingosylphosphocholine (NBD-SM), 1-Acyl-2-[6-[(7-nitro-2-1,3-benzoxadiazol-4-yl)amino] caproyl]-*sn*-glycero-3-phosphatidylserine (NBD-PS), 25-[*N*-[(7-nitro-2-1,3-benzoxadiazol-4-yl)methyl]amino]-27-norcholesterol (NBD-Ch). Beltsville thawing solution with (BTS+) and without antibiotics (BTS) was obtained from Minitüb GmbH (Tiefenbach, Germany). Propidium iodide (PI) was purchased from Invitrogen Life Technologies GmbH (Darmstadt, Germany). Agarose with a gelling temperature of 36 ± 1.5 °C for immobilization of the sperm was obtained from Carl Roth GmbH + Co. KG (Karlsruhe, Germany).

Labeling of sperm

Sperm-rich ejaculate fractions were collected from fertile boars (*Sus scrofa domestica*, race Piétrain or Duroc) in accordance with the rules on the care and use of domestic animals at commercial boar stations in Brandenburg (Germany). The ejaculates were diluted to a final concentration of 2.2 × 10^8 sperm/ml with BTS+ composed of 10 mM KCl, 20.4 mM trisodium citrate, 15 mM $NaHCO_3$, 3.36 mM EDTA, 205 mM glucose, and antibiotics, and prewarmed to 38 °C. The prepared sperm were then gradually

cooled, transported, and stored at 17 °C until use within 24 h after collection. An amount of 12.5 ml of diluted boar ejaculate was transferred into Falcon tubes and incubated for 10 min at 38 °C followed by 6-min centrifugation at 750×*g* at room temperature with reduced acceleration and deceleration (accel/decel 4/4, Biofuge Stratos, Heraeus). The pellet was carefully resuspended in 1 ml BTS, transferred into a 1.5-ml Eppendorf tube and centrifuged at 500×*g* at room temperature (Biofuge fresco, Heraeus). The pellet was resuspended in 100 µl of BTS containing approximately 2.4 × 10^8 sperm. All subsequent measurements were performed within 3 h to preserve a high viability of the sperm.

NBD-labeled lipids were stored as chloroform solutions at −20 °C. For usage, the chloroform was evaporated in a nitrogen flow and the NBD-labeled lipids were dissolved in BTS as stock solutions by mixing with a vortex. In case of NBD-PS and NBD-SM, the stock solutions had a concentration of 400 µM. Labeling of cells with NBD-Ch was performed by using methyl-β-cyclodextrin. The NBD-Ch stock solution consisted of 36 µM NBD-Ch, 1 mM methyl-β-cyclodextrin, and 500 µM cholesterol in order not to modify the cholesterol content of the cells during labeling. Cells were labeled by mixing 50 µl of sperm suspension with 10 µl (NBD-SM, NBD-PS) or 50 µl (NBD-Ch) of the stock solutions followed by an incubation in the dark at room temperature for 5 min (NBD-SM) or 15 min (NBD-PS, NBD-Ch). Subsequently, 1 ml of BTS was added and cells were washed by centrifugation (6 min, 500×*g*, room temperature). The resulting pellet was resuspended in 50 µl of BTS.

Ten microliters of the labeled sperm was mixed with 500 µl BTS solution and, for FLIM measurements, 2.5 µl PI. PI served as a marker for non-vital cells. Agarose solution (0.5 % in BTS) was melted by cooking, cooled down to 38 °C, and mixed with the prewarmed (38 °C) NBD- and PI-labeled sperm. A total of 7.5 µl of the mixture was applied on an object slide for the measurements. Cooling the slide to room temperature triggered gelation of the agarose and therefore, an immobilization of embedded sperm, which allowed to perform the fluorescence measurements. Even at 38 °C the sperm were sufficiently immobilized due to the high viscosity of the fluid agarose. Because of the potential cytotoxicity of PI, the sperm were used for a maximum of 30 min after PI staining.

The FLIM, FRAP, and FCS measurements were carried out at ambient room temperature (RT, 26.3 ± 1.5 °C). FLIM measurements were additionally performed in a tempered acrylic glass box at 38 °C to examine the extent of temperature-related changes of fluorescence lifetime upon cooling to RT. Chromatographic analyses of organic sperm extracts revealed that the enzymatic degradation of NBD-PS as well as NBD-SM was negligible in the time frame of the experiments (not shown).

Analysis of transversal membrane distribution of NBD-cholesterol

Sperm were labeled by NBD-Ch as described above (15-min incubation with NBD-Ch followed by centrifugation and resolution of the cell pellet). Twenty, 45, and 65 min after the start of the labeling procedure, an aliquot of the resolved pellet (10 µl) was transferred into 240 µl of BTS at 38 °C and after addition of 2.5 µl PI incubated for 5 min. An aliquot of stained sperm suspension (~0.25 × 10^6 sperm) was diluted in 2 ml BTS at 38 °C for measurement in a flow cytometer (CyFlow space and Flowmax software, Partec, Germany) equipped with a 50-mW solid-state laser (Ex 488 nm), a 515–560-nm band-pass for NBD (green), and a 620-nm long-pass filter for PI (red). The system was triggered on the forward light scatter, and 15,000 cells per sample were characterized for their fluorescence at a flow rate of about 250 cells per second. After gating sperm signals by forward and sideward light scatter, mean intensity of NBD fluorescence was determined for vital and non-vital (PI-positive) cells. The measurement was repeated in the presence of 25 mM sodium dithionite added from a cold stock solution (1 M in 100 mM Tris-buffer, pH 10). The initial quenching of accessible NBD-Ch molecules, i.e., decrease of fluorescence intensity, was recorded after 0.5-min co-incubation with dithionite and the progressive quenching of NBD fluorescence with time was followed. A previous experiment revealed that the extent of initial quenching was not increased by using higher dithionite concentrations up to 50 mM (see Supplementary Fig. 1, insert).

FLIM measurements

To determine the fluorescence lifetimes of NBD analogs in the sperm membrane, time-correlated single-photon counting was performed using an inverse FluoView 1000 microscope (Olympus, Tokyo, Japan) with an oil objective (60×/1.35) for confocal laser scanning microscopy supplemented with a commercial FLIM upgrade kit from PicoQuant (Berlin, Germany). The excitation laser was a pulsed diode laser with a wavelength of 468 nm (pulse length 60 ps, pulse frequency 10 MHz, 4 µs/pixel). The emission was detected by an avalanche photodiode (APD) after passing a 540/40 band pass filter. Pictures were collected with a frame size of 512 × 512 pixels. Sixty frames were collected for every data set. The photon count rate varied between 1 × 10^3 and 1 × 10^5 counted photons/s. Pseudocolored pictures were created with the average lifetime per pixel (2 × 2 binning). The summed-up number of photons per

pixel (2 × 2 binning) revealed the picture of fluorescence intensity.

The recorded pictures were analyzed using Olympus FluoView FV1000 software to document sperm morphological integrity and vitality by PI staining. Acrosomal and postacrosomal head regions were manually selected as regions of interest (ROIs). For each ROI, an overall fluorescence decay curve was generated by summing up the photons registered for that region. The width of the bins of the decay histogram was chosen as 30.5 ps. To determine the fluorescence lifetimes by a non-linear least-squares iterative fitting procedure, FLIM data sets were loaded into the software SymphoTime (Analysis) 4.7.2 according to Stöckl et al. (2008).

The decay curves could be principally fitted by two components giving two lifetimes. The shorter lifetime of approximately 2 ns was not considered (Klein et al. 2012; Stöckl et al. 2008). This component represents a comparatively small amount of fluorophores and we assume that these fluorophores, due to a back-loop of their NBD-labeled fatty acyl chains (Chattopadhyay 1990), have access to extra- or intra-cellular aqueous surroundings. Therefore, the very short lifetime probably does not reflect the properties of the respective membrane leaflet under investigation. This assumption is supported by the fact that the fluorescence lifetime of NBD is reduced to 0.9 ns in water, while being in the range of 7–10 ns in aprotic solvents (Lin and Struve 1991). A typical lifetime histogram and fitted data for the two head regions of a NBD-SM labeled sperm cell are shown in Supplementary Fig. 2.

FRAP measurements

FRAP was used to evaluate the diffusion coefficient (D) of NBD-SM, NBD-PS, and NBD-Ch in the sperm head membrane by selecting circular ROIs in its acrosomal and postacrosomal region. We note that the fluorescence intensity in the postacrosomal region of the sperm head was remarkably low for NBD-Ch.

The measurements were performed using a LSM-710ConforCor3 system (Carl Zeiss Microscopy, Jena, Germany) equipped with an argon laser (488 nm), a main beam splitter MBS 488, an emission META detector (34 PMTs, 505–650 nm), and an oil immersion objective (100×/1.4). The data were recorded by ZEN2010 software (Carl Zeiss MicroImaging, Jena, Germany) using a time series consisting of 400 images, time interval of 25 ms, bleaching after the 10th image (25 iterations 300 ms, laser power 100 times stronger than the imaging performance).

The attained FRAP data were processed with Prism (Version 5.01, 2007, GraphPad) by fitting to a biexponential decay curve [see formula (1)] to evaluate the half-time of fluorescence recovery ($t_{½}$).

$$I(t) = A_1 + (B_1 - A_1)\, e^{-t/T_1} + A_2 + (B_2 - A_2)\, e^{-t/T_2} \tag{1}$$

To obtain D, the formula (2) was used with w representing the radius of the ROI in case of an uniform disc bleaching profile (Axelrod et al. 1976):

$$D = \gamma_D \frac{w^2}{4\tau_{1/2}} \tag{2}$$

Due to the fact that the region of interest was stimulated by a series of laser spots, with a diameter of seven pixels, w was calculated to a value of 0.343 µm. γ_D is a factor corresponding to the beam shape, type of transport, and bleaching parameter. For uniform bleaching of a circular disc and a fluorescence recovery dominated by lateral diffusion, this parameter can be estimated as 0.88 (Axelrod et al. 1976). Since in our case the ROI was bleached by a series of laser spots instead a uniform disc bleaching profile, the true bleaching profile resembles more an uniform disc with Gaussian edges (Braga et al. 2004) and therefore, the assumption for γ_D might be suboptimal, but deviations in this factor should have only a minor influence on the resulting D.

A typical decay curve and fitted data for the two head regions of a NBD-SM labeled sperm cell are shown in Supplementary Fig. 3.

FCS measurements

FCS measurements were performed at room temperature on a LSM710-ConfoCor3 system (Carl Zeiss Microscopy GmbH, Jena, Germany). NBD fluorescence signals were recorded after excitation by an argon laser (488 nm) using a water objective (40×/1.2) and a main beam splitter MBS488, through a 505-nm longpass filter. Membranes were located by z-scans. Intensity fluctuations were recorded for 4 s and 25 repetitions and further data analysis was carried out using the ZEN 2010 software (Carl Zeiss Microscopy GmbH, Jena, Germany) which also calibrated the PSF. An auto-correlation curve was derived for each raw data set by applying the following formula:

$$G(\tau) = 1 + \frac{\langle \delta F(t)\, \delta F(t+\tau) \rangle}{\langle F(t) \rangle^2} \tag{3}$$

where $\langle\ \rangle$ denotes averaging over time and $\delta(x)$ is an abbreviation of $x - \langle x \rangle$. The correlation curves were fitted using a two-component model of free diffusion in two dimensions with triplet fraction and an offset for membrane-associated proteins (Teichmann et al. 2014) analytically given by

Table 1 Quenching of NBD-labeled lipid analogs for cholesterol (Ch) in the boar sperm membrane by sodium dithionite

Time after start of NBD-Ch labeling (min)	Non-vital	+Dithionite		Vital	+Dithionite	
	% of sperm	% of sperm	% quenching	% of sperm	% of sperm	% quenching
25	65.3 ± 6.5	66.3 ± 4.0	96.8 ± 0.7	34.7 ± 5.6	33.7 ± 4.0	55.0 ± 1.4
50	43.3 ± 15.2	42.9 ± 18.0	96.2 ± 1.3	56.7 ± 15.2	57.1 ± 18.0	50.0 ± 5.2
70	54.6 ± 14.0	49.1 ± 12.8	96.6 ± 0.5	45.4 ± 14.0	50.9 ± 12.8	51.7 ± 5.8

Vital and non-vital boar sperm cells were discriminated by propidium iodide and analyzed by flow cytometry for their NBD fluorescence at different times after labeling with NBD-Ch. The amount of label accessible towards dithionite was determined 0.5 min after addition of 25 mM dithionite to the sperm cells. Means and standard deviations are given ($n = 3$)

$$G(\tau) = 1 + G_\infty + \frac{1}{N}\left(1 + \frac{T \times e^{-\tau/\tau_T}}{1-T}\right) \times \left(\frac{1}{\left(1+\frac{\tau}{\tau_{D1}}\right)} + \frac{1-f}{\left(1+\frac{\tau}{\tau_{D2}}\right)}\right) \quad (4)$$

where G_∞ is the offset from one. N and T represent the total number of particles and the triplet fraction, respectively. The free diffusion times are represented by τ_{D1} andτ_{D2} (the subscripts indicate the different molecule species). τ_T is the triplet time, f and $1 - f$ are the fractions of species one and two and τ is the correlation time. The first component was too fast to reflect membrane diffusion and likely reflects a protonation kinetic of the fluorescent molecules leading to blinking (Haupts et al. 1998). Thus the diffusion time of the second component was considered to be significant (Elson 2001). Finally, all data sets with convergent fit results out of the 25 recorded were averaged.

Diffusion coefficients were calculated from the obtained diffusion times by the formula

$$D = \frac{\omega^2}{4 * \tau} \quad (5)$$

where ω represents the radius of the confocal volume and τ is the characteristic diffusion time.

A typical autocorrelation curve and fitted data for the two head regions of a NBD-SM labeled sperm cell are shown in Supplementary Fig. 4.

Statistics

Significances were tested using the open-source software R 2.15. Acrosome and postacrosome were compared using a paired Wilcoxon signed-rank test while a Mann–Whitney U test was applied to compare different temperatures, vitalities, and analogs in the same sperm region.

Results

Analysis of transversal membrane distribution of NBD-cholesterol

Although there are many data supporting an even distribution of cholesterol and its analogs between both membrane leaflets in several plasma membranes (Müller et al. 2011), such a distribution has not been shown for sperm cells so far. Therefore, a dithionite-based assay was applied to analyze the transversal distribution of fluorescent cholesterol analogs at different times after their incorporation in the boar sperm membrane. Immediately after the addition of 25 mM dithionite to labeled sperm, about 50 % of the NBD fluorescence in vital and about 97 % in non-vital (PI-positive) cells was quenched without influence on the proportion of vital sperm (Table 1). This implies that 50 % of the NBD-Ch in vital cells is accessible for the extracellular quencher and, obviously, located in the outer membrane half. This transversal distribution of NBD-Ch was observed for the whole time period in which labeled sperm were used for analysis by FLIM, FRAP, and FCS (25–70 min after start of labeling, Table 1).

Upon extended incubation in the presence of dithionite (up to 20 min), the NBD-Ch fluorescence in vital sperm was progressively quenched to values comparable to those in non-vital cells (Supplementary Fig. 1) while the amount of vital sperm was reduced by 10 % at most. A progressive permeation of dithionite through the membrane of PI-negative cells would inevitably result in a loss of sperm vitality and concomitant incorporation of PI. The latter was observed after addition of 0.5 % Triton X-100 (data not shown). Therefore, the reason for the progressive quenching might rather be a flipping of NBD-Ch between both membrane leaflets, exposing initially inaccessible molecules to the quencher outside the cell.

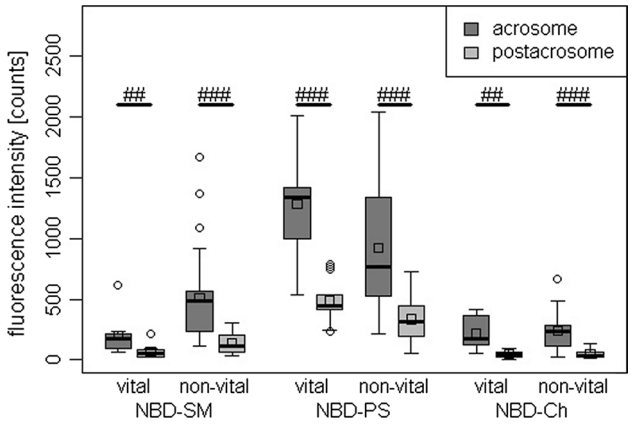

Fig. 2 Fluorescence intensities of NBD-labeled lipid analogs for sphingomyelin (SM), phosphatidylserine (PS), and cholesterol (Ch) incorporated in the acrosomal (*dark grey*) and postacrosomal (*light grey*) membrane regions of vital and non-vital boar sperm cells derived from FLIM measurements at 38 °C. Means and standard errors of means are shown (R 2.15). Values were corrected for the different size of both regions (see "Materials and methods"). Significant differences between regions (paired Mann–Whitney *U* test) are indicated ($^{\#}p < 0.05$, $^{\#\#}p < 0.01$, $^{\#\#\#}p < 0.001$). Different fluorescence intensities were observed between vital and non-vital sperm by Mann–Whitney *U* test (NBD-SM, acrosomal region: $p < 0.01$, postacrosomal region: $p < 0.05$; NBD-PS, acrosomal region: $p < 0.05$, postacrosomal region: $p < 0.01$). Significant differences between NBD-SM and NBD-PS as well as between NBD-PS and NBD-Ch (Mann–Whitney *U* test) in vital cells were found in both regions ($p < 0.001$)

FLIM measurements

Fluorescence lifetime imaging was applied to visualize the distribution of fluorescence lifetimes for the different NBD-labeled lipid analogs in single vital sperm after co-staining the cells with PI. FLIM was performed at room temperature (RT) and at 38 °C.

Fluorescence intensities of the cells recorded during FLIM measurements were used to verify the incorporation of the lipid analogs into sperm. Summarized intensity values for pixels in defined ROIs were normalized to the respective areas. The fluorescence intensity should correlate to the amount of analog incorporated into the membrane assuming that no bleaching occurs at the given label concentrations. All analogs incorporated to a higher extent into the acrosomal compared to the postacrosomal region (Fig. 2). Sperm labeled with NBD-SM and NBD-Ch were only weakly fluorescent compared to sperm labeled with NBD-PS. NBD-SM incorporation increased in non-vital compared to vital cells which was also found for $DiIC_{12}$ (James et al. 1999). These authors assume that in non-vital cells also underlying organelles become stained because of cell membrane ruptures. This seems, however, not to be the case for NBD-Ch and NBD-PS, whose intensities are similar or even lower in non-vital sperm, respectively. In case of NBD-PS, non-vital cells do not actively translocate the analogs to the cytoplasmic membrane half during the labeling procedure. They are obviously not spontaneously included in the exposed leaflet of underlying membranes. The latter also applies to NBD-Ch and was confirmed by the intensity data revealed by flow cytometry for vital and non-vital sperm in the dithionite assay (not shown).

Representative pseudocolored images as well as fluorescence lifetime data of vital (PI-negative) cells are shown in Figs. 3 and 4. Differences of fluorescence lifetimes between sperm head and tail regions are obvious in Fig. 3. However, the number of photon counts per area was insufficient in the sperm tail. Therefore, only data from both head regions were determined and presented in Fig. 4. For all following considerations, it is important to note that the fluorescence intensity in the postacrosomal region of NBD-Ch-labeled cells was rather low and that the data obtained for this label and region should be regarded with caution.

All fluorescence lifetimes measured at 38 °C were lower compared with the respective data for analog and sperm region at RT, which is in agreement with a previously published dependence of NBD fluorescence lifetime on temperature (Fery-Forgues et al. 2003). This temperature effect was—with a difference of about 2 ns—most pronounced for NBD-SM.

When compared to NBD-PS, fluorescence lifetimes at 38 °C were significantly higher for NBD-Ch and in the acrosomal region also for NBD-SM. At RT, NBD-PS showed the lowest fluorescence lifetimes, highest values were measured for NBD-SM followed by NBD-Ch. The most pronounced lifetime variability between both temperatures was detected for NBD-SM.

Comparing the results between both sperm head regions, significantly higher fluorescence lifetimes were determined in the acrosomal region with the exception of NBD-SM showing no differences between both sperm head regions. The largest differences of fluorescence lifetimes between acrosomal and postacosomal region were observed for NBD-Ch (Fig. 4). Note, that data evaluation by exponential fitting procedures (see "Materials and methods") revealed, besides a component with a very low lifetime (which was neglected, see "Materials and methods"), no indication for the co-existence of clearly distinct label populations with different lifetimes within one region. However, the lifetime distributions in each head region were relatively broad, particularly for NBD-SM (Δ about 3–4 ns, Fig. 3).

FRAP measurements

FRAP measurements were performed in the acrosomal and postacrosomal region of sperm and diffusion coefficients (*D*) for the NBD-labeled lipid analogs were determined from the recovery curves. In the acrosomal region,

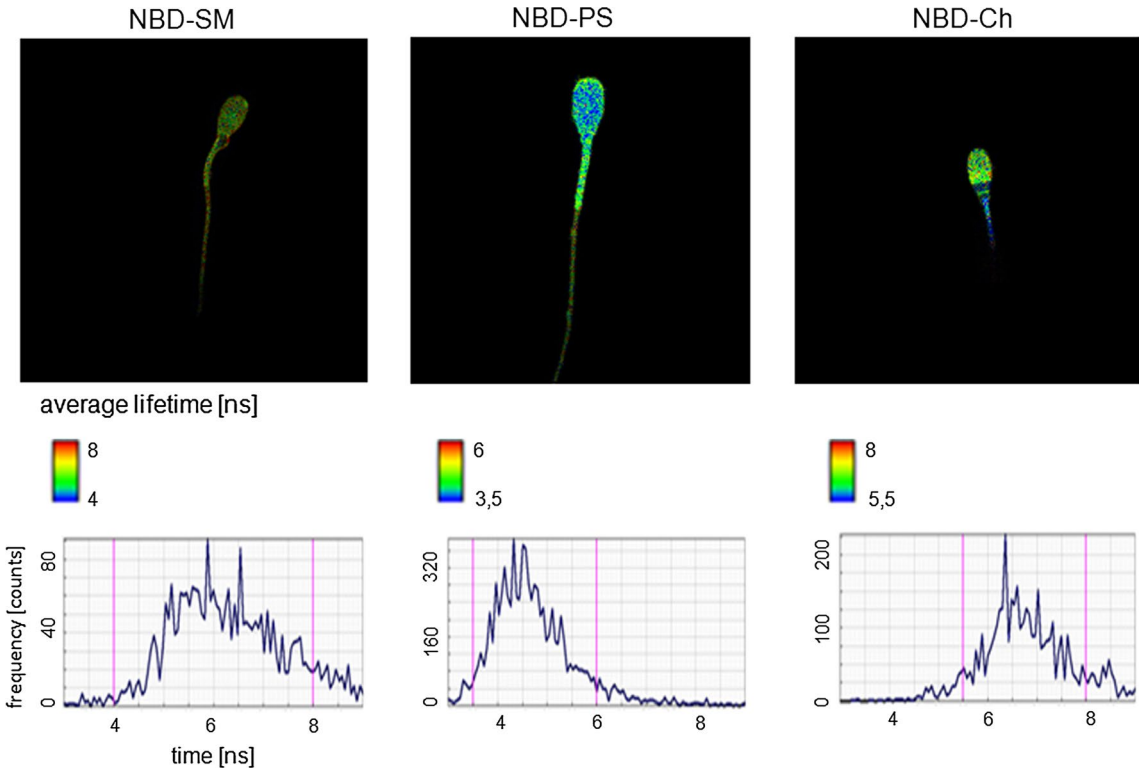

Fig. 3 Fluorescence lifetime images and histograms of NBD-labeled lipid analogs for sphingomyelin (SM), phosphatidylserine (PS), and cholesterol (Ch) incorporated in the membranes of vital domestic boar spermatozoa. FLIM measurements were performed at 38 °C. Average lifetime is shown as pseudocolor image (see *scale*). *Pink colored lines* in the histograms mark the borders of *color coding* of the FLIM images

diffusion coefficients of all three analogs were similar with values of around 1.5×10^{-9} cm^2/s (Fig. 5). Comparing the two sperm head regions, D values of NBD-SM as well as NBD-PS were significantly lower (by about 50 %) in the postacrosomal compared to the acrosomal region. No difference between these regions was found for NBD-Ch. Therefore, diffusion of NBD-Ch in the postacrosomal region was faster compared to NBD-SM and NBD-PS.

FCS measurements

Diffusion coefficients of NBD-labeled lipids were also determined from FCS measurements revealing a different picture (Fig. 6). Generally, much higher (by a mean factor of 45) *D* values were found in FCS compared to FRAP measurements. No differences were observed between acrosomal and postacrosomal region for all three lipid analogs, contradictory to the results obtained by FRAP using NBD-SM or NBD-PS. The postacrosomal *D* values of NBD-Ch were significantly lower than those of NBD-PS. A conspicuously large inter-cellular variability of *D* was found for NBD-PS in both regions.

Discussion

In the present study, the behavior of different fluorescent lipid analogs in the acrosomal and in the postacrosomal region of ejaculated boar sperm was characterized by various approaches of fluorescence microscopy. During transit of sperm through the female genital tract, the acrosomal region interacts with the epithelial cells from the oviduct, e.g., forming a sperm reservoir and supporting sperm capacitation as a prerequisite to fertilization. Moreover, the acrosomal region provides the structures and components that mediate the first contact to the *zona pellucida*, which is the main stimulus for the acrosome reaction enabling the sperm penetration through the oocyte-surrounding layer. While the anterior part of the sperm head is destroyed during acrosome reaction, the postacrosomal region is important for maintaining cell stability via connections to underlying cytoskeletal components (Jamil 1984), but is also the region of initial contact and subsequent fusion with the oocyte membrane (Ikawa et al. 2010).

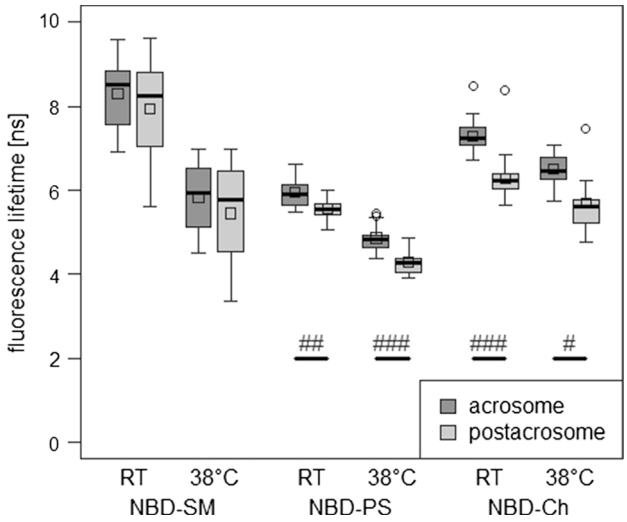

temperature	*RT*		*38°C*	
region	*acrosomal*	*postacrosomal*	*acrosomal*	*postacrosomal*
NBD-SM versus NBD-PS	***	***	**	***
NBD-SM versus NBD-Ch	**	**	-	-
NBD-PS versus NBD-Ch	***	***	***	***

Fig. 4 Fluorescence lifetimes of NBD-labeled lipid analogs for sphingomyelin (SM), phosphatidylserine (PS), and cholesterol (Ch) incorporated in the acrosomal (*dark grey*) and postacrosomal (*light grey*) membrane regions of vital domestic boar sperm cells. FLIM measurements were performed at room temperature (RT; NBD-SM: $n = 8$, NBD-PS: $n = 9$, NBD-Ch: $n = 32$) and at 38 °C (NBD-SM: $n = 11$, NBD-PS: $n = 13$, NBD-Ch: $n = 9$). Data are displayed by means of boxplots (R 2.15). Medians and the 10th, 25th, 75th, and 90th percentiles are shown as *vertical boxes* with *error bars*, outliers are denoted by *open circles* and means are shown as *small squares*. Significant differences between regions (paired Mann–Whitney *U* test) are indicated ($^{\#}p < 0.05$, $^{\#\#}p < 0.01$, $^{\#\#\#}p < 0.001$). For each distinct region and analog, fluorescence lifetimes were lower at 38 °C compared to RT (Mann–Whitney *U* test, $p < 0.01$). Significant differences between analogs (Mann–Whitney *U* test) are presented in Table:

FLIM measurements

With the increasing knowledge on comparably stable substructures within membranes, so-called rafts, constituted by certain lipids (essentially Ch and SM) and proteins with a high affinity for interaction in liquid-ordered domains (Simons and Gerl 2010), the analysis of these temporally and spatially organized units came increasingly into the focus of cellular investigations. With regard to the physicochemical properties within the domains, it is assumed that lipid subpopulations captured in those structures exhibit a restricted diffusion compared to freely fast-diffusing lipids outside the structures. They could also be limited in their interaction with surrounding molecules, which would affect the fluorescence lifetime of incorporated fluorescent markers.

The NBD fluorophore is a very subtle sensor of environmental changes since various spectral properties including its fluorescence lifetime are strongly dependent on solvent polarity and the presence of hydrogen donors (Fery-Forgues et al. 2003). While the fluorescence lifetime of NBD is in the range of 7–10 ns in non-polar aprotic solvents, its fluorescence lifetime is reduced to 1 ns in the polar, strongly protic solvent water. The reason for this behavior was attributed to a strongly increased rate of non-radiative deactivation in more polar and protic solvents (Fery-Forgues et al. 2003; Lin and Struve 1991). NBD-labeled lipid analogs have been successfully applied to analyze the membrane properties both in model membranes (Stöckl et al. 2008) and living cells (Klein et al. 2012; Mukherjee et al. 2006; Ostasov et al. 2013). Even though NBD-labeled lipids, like any analog, may reflect physical properties of endogenous lipids in some cases only to a certain extent (Chattopadhyay 1990), they have been proven to faithfully reflect the transversal distribution of endogenous lipids in sperm (Gadella et al. 1999; Kurz et al. 2005; Müller et al. 1994; Nolan et al. 1995) and were successfully applied to analyze membrane environments using their longer fluorescence lifetime (Klein et al. 2012; Stöckl et al. 2008). Since it has been shown in model membranes that the fluorescence lifetime of markers like NBD-labeled lipids is not the same in different lipid domains (Stöckl et al. 2008), FLIM

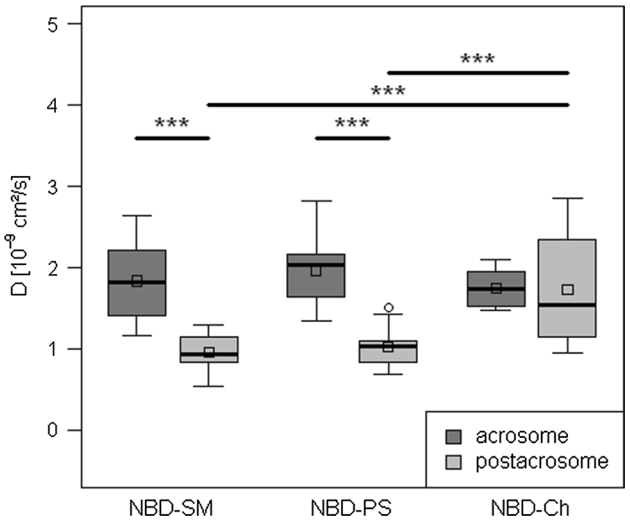

Fig. 5 Diffusion coefficients (*D*) of NBD-labeled lipid analogs for sphingomyelin (SM), phosphatidylserine (PS), and cholesterol (Ch) localized in the acrosomal (*dark grey*) and postacrosomal (*light grey*) membrane regions of domestic boar sperm heads calculated from FRAP measurements (NBD-SM: $n = 37/34$, NBD-PS: $n = 15/11$, NBD-Ch: $n = 7/8$). Data are displayed by means of boxplots (R 2.15). Medians and the 10th, 25th, 75th, 90th percentiles are shown as *vertical boxes* with *error bars*, outliers are denoted by *open circles* and means are shown as *small squares*. Significant differences either between regions or analogs (Mann–Whitney *U* test) are indicated (*$p < 0.05$, **$p < 0.01$, ***$p < 0.001$)

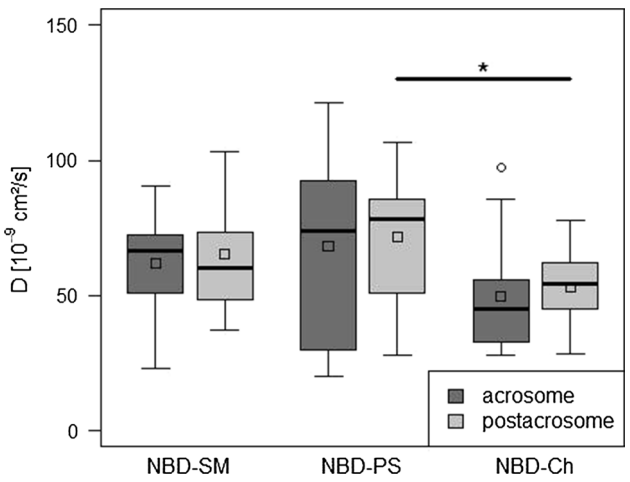

Fig. 6 Diffusion coefficients (*D*) of NBD-labeled lipid analogs for sphingomyelin (SM), phosphatidylserine (PS), and cholesterol (Ch) localized in the acrosomal (*dark grey*) and postacrosomal (*light grey*) membrane regions of domestic boar sperm heads calculated from FCS measurements (NBD-SM: $n = 12/14$, NBD-PS: $n = 17/17$, NBD-Ch: $n = 13/13$). Data are displayed by means of boxplots, (R 2.15). Medians and the 10th, 25th, 75th, and 90th percentiles are shown as *vertical boxes* with *error bars*, outliers are denoted by *open circles* and means are shown as *small squares*. Significant differences either between regions or analogs (Mann–Whitney *U* test) are indicated (*$p < 0.05$, **$p < 0.01$, ***$p < 0.001$)

analyses of NBD analogs were performed in the discrete (acrosomal and postacrosomal) sperm head regions.

FLIM allows a fast, high-resolution measurement of the complete areas of both head regions in vital sperm. Decay curves of fluorescence intensity could be properly fitted with two lifetime components for each analog in both membrane compartments. We solely used the higher lifetime, which characterizes the motional freedom of the NBD-label of the respective lipid analog and surrounding solvent molecules (see "Materials and methods"). Since we observed no further pronounced analog population having a different lifetime, we assume that the analogs in the acrosomal as well as in the postacrosomal region are not organized in substructures clearly distinguishable by their influence on fluorescence lifetimes. FLIM analyses of NBD-PC and NBD-PS in cell membranes of HepG2- and HeLa-cells could also not resolve distinct domain specific lifetimes (Stöckl et al. 2008). An overlapping broad lifetime histogram centered on lifetimes corresponding to values detected for liquid-ordered domains in artificial membranes was revealed (11.5 ns for NBD-PC, 10.9 ns for NBD-PS at 25 °C). If domains exist in these cell types, the cell membrane seems to consist of a variety of lipid domains differing in properties like composition, size, and stability (Stöckl et al. 2008). Moreover, it is assumed that native cell membranes create a rather continuous liquid-ordered phase with embedded small disordered domains (Almeida et al. 2005; Mukherjee and Maxfield 2004). Also in boar sperm, broad lifetime histograms were revealed per region, however, even at room temperature (26 °C) values never exceed 10 ns. In giant unilamellar vesicles (GUVs) of lipid mixtures known to form ordered and disordered domains as well, lifetimes of 12 and 7 ns were resolved for NBD-PC at 25 °C, respectively (Stöckl et al. 2008). We conclude that lifetimes of all NBD analogs in the boar sperm head rather correspond to those in disordered domains and are much lower when compared to HepG2 and HeLa cells. This has important implications for the functionality of mammalian sperm, which need to sustain their fusogeneity for the exocytotic acrosome reaction (acrosomal region) and fusion with the oocyte (postacrosomal region). This suggests a strong need for stabilization of sperm membranes before fertilization by proteins or binding to oviduct.

As outlined in the introduction, the NBD analogs used here allow to selectively sense the leaflets of the sperm membrane. The localization of more than 95 % NBD-PS on the inner membrane leaflet as well as of more than 95 % NBD-SM on the outer membrane leaflet is well documented in the literature (Gadella et al. 1999; Kurz et al. 2005; Müller et al. 1994; Nolan et al. 1995) and can be presumed in both large head regions. For NBD-Ch, we could confirm here for sperm that it is indeed symmetrically distributed across both membrane leaflets and shows a rapid

flip-flop across the bilayer (Müller et al. 2011). However, we cannot exclude that the transversal distribution and mobility of NBD-Ch differs between the macrodomains of the head. Furthermore, the fluorescence of the NBD group is amongst others sensitive to the polarity and hydrogen-bonding donor strength of its surroundings, therefore being able to sense even small differences between different membrane substructures.

Comparing the lifetimes of the three different analogs, NBD-PS showed the shortest lifetimes at body as well as at room temperature. This is in agreement with the assumption of a more fluid cytoplasmic membrane leaflet in eukaryotic cells (Julien et al. 1993; Seigneuret et al. 1984). Because NBD-PS as well as endogenous PS is rapidly transported to the cytoplasmic leaflet in vital boar sperm it is nearly exclusively located on that membrane half under our experimental conditions (Kurz et al. 2005; Müller et al. 1994). Similar to the lifetime measurements, NBD-PS also tends to have a larger diffusion mobility reflected by highest average diffusion coefficients deduced from FCS in both head compartments. When the temperature was reduced from 38 °C to room temperature, the lifetime of all analogs increased. However, this increase varied for the analogs suggesting a different behavior/reorganization of each analog within the membrane. The largest increase was observed for NBD-SM in the outer leaflet and comes nearest to values in liquid-ordered domains in GUVs (see above). It remains open whether the smaller response to temperature change of NBD-Ch is explained by its particular arrangement in the membrane or by a reduced temperature sensitivity of the particular type of NBD bonding compared to chain-labeled analogs (Fery-Forgues et al. 2003). Notably, the variation of lifetimes between single sperm was remarkably high for NBD-SM compared to NBD-Ch or NBD-PS. The induced changes upon cooling could be relevant for stabilizing reorganization processes during sperm storage at slightly lower temperature in the epididymis. This would additionally have implications for low-temperature sperm storage before artificial insemination which could in future be investigated by NBD analogs in similar approaches.

The existence of liquid-ordered membrane (raft) domains has been postulated for boar sperm after analyzing functional protein complexes like for instance GM1 related domains (typical raft marker) in detergent resistant membrane fractions by several authors (Boerke et al. 2008; Bou Khalil et al. 2006; Jones et al. 2010; Peterson et al. 1987; Tanphaichitr et al. 2007; van Gestel et al. 2005). However, for no type of NBD analog did FLIM analyses reveal clearly distinguishable coexisting lipid populations, comparable to liquid-ordered and -disordered domains, within one head region. At least for NBD-Ch it is not sure if the analog locates to liquid-ordered and -disordered domains as well, since it has been shown for artificial membranes that NBD-PC and NBD-Ch, like the majority of fluorescent lipid analogs, accumulate predominantly into the liquid-disordered phase. For NBD-SM, conflicting data have been published (Ramstedt and Slotte 2006; Sengupta et al. 2008; Sezgin et al. 2012; Wang and Silvius 2000, 2003). Therefore, we have characterized the lateral arrangement of NBD-SM in phase-separated GUVs finding that about 75 % of this analog are localized in the liquid-ordered domain (see supplementary information).

Comparing both large sperm head regions, fluorescence lifetimes of NBD-PS and NBD-Ch are higher in the acrosomal than in the postacrosomal part. This means that the probability of molecular interactions of NBD-groups (as a possible consequence of their motional freedom in a suggested more fluid or aqueous environment) is higher in the postacrosomal region and concerns particularly analogs with partition into the cytoplasmic leaflet. Whereas close membrane contact as prerequisite for fusion (acrosome reaction) might restrict mobility in the acrosomal part of the head, different conditions in the posterior head region might be required for later reorganization of postacrosomal proteins upon capacitation/acrosome reaction as demonstrated for bovine and human sperm (Howes et al. 2001; Luconi et al. 1998).

Discrepancies between FRAP and FCS measurements

Comparing our data on analog diffusion obtained from FRAP and FCS measurements, the diffusion coefficients as well as the ratio of diffusion coefficients between the two sperm head regions strongly differ in dependence of the detection method used. This indicates that the apparent value of diffusion coefficients (D) depends on the temporal and spatial scale of the measurement.

Similar discrepancies have been described elsewhere recently. Similar to our data on lipids, Adkins et al. (Adkins et al. 2007) detected a tenfold difference in diffusion coefficients calculated from FRAP and FCS measurements for a membrane protein (tagged with yellow fluorescent protein) in HEK293 cells. The authors assumed an overestimation of D values by FCS measurements. Guo et al. (2008) compared different fluorescence techniques to analyze fluorescent lipid analogs in supported lipid bilayers and GUVs. Again, diffusion coefficients calculated from FRAP were significantly lower than those calculated with FCS. Since their FCS data were in better agreement with diffusion coefficients obtained from single particle tracking (SPT) in supported lipid bilayers where D values are determined from real diffusion pathways of multiple discrete molecules, the authors rather assumed an underestimation of D values by FRAP.

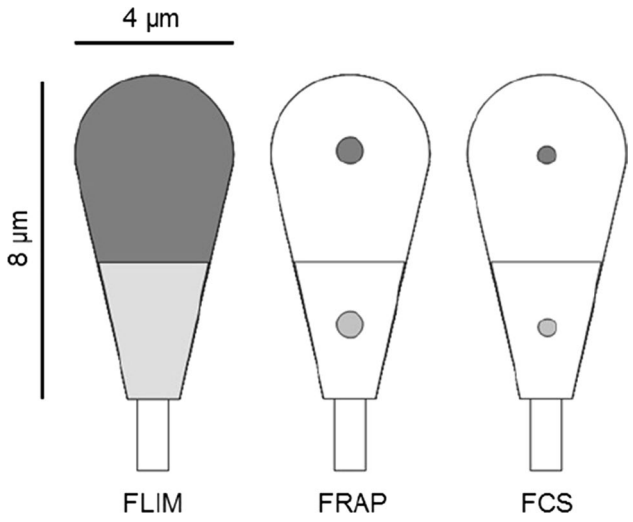

Fig. 7 Visualization of membrane dimensions and measurement parameters of the different methods characterizing the behavior of fluorescently labeled lipid analogs localized in membrane regions of domestic boar sperm heads. For further explanation on the applied methods (FLIM, FRAP with different bleach spot sizes, FCS), see the "Introduction". *Colors* indicate the measured share of the acrosomal (*dark grey*) and postacrosomal (*light grey*) region

In accordance with the latter authors, we hypothesize that the FRAP measurements in our study also caused a significant underestimation of diffusion velocity compared to FCS-derived data. Already in the past, some groups challenged the applicability of conventional FRAP formulas (that were derived for static bleaching lasers) in confocal laser scanning microscopy (CLSM) as presented by (Axelrod et al. 1976), and found that the diffusion of molecules between bleach spot and surrounding membrane during the bleaching interval leads to a significant increase in the effective bleach spot size (bleach spot broadening) and cannot be neglected when using CLSM in FRAP experiments (Braga et al. 2004; Kang et al. 2009, 2012). This increase in effective bleach spot size finally causes an underestimation of the diffusion coefficient when conventional data analysis is performed on the recovery data collected. The effect is more pronounced for longer bleaching times, small bleach spots, and high diffusion coefficients. Note that due to the scanning nature of the bleaching laser beam in CLSM, an increase in bleach spot size is accompanied by an increase in bleaching time and vice versa, which makes it difficult to avoid this aberration. If the labeled marker species consists of subspecies that diffuse with different velocities, these subspecies are differentially influenced by the increase in effective bleach spot size. The kinetics of the recovery curve may then be dominated by slower moving molecules.

Previous FRAP measurements on boar sperm used static lasers with Gaussian profile to create a bleach spot with a diameter of 1.2 or 2.5 µm after 5-ms bleaching time. For the artificial lipid reporter ODAF, D values of about 30×10^{-9} cm^2 s^{-1} were reported for both boar sperm head regions at 23 or 25 °C (James et al. 1999; Wolfe et al. 1998). James et al. found D values of about 70 and 50×10^{-9} cm^2 s^{-1} for another lipid-like reporter (DiIC$_{12}$) in the acrosomal and postacrosomal region, respectively (James et al. 2004). Note that the mentioned underestimation of D is negligible in these FRAP protocols. Yet the size of these bleach spots seems inadequate to the size and geometry of the sperm head, particularly of the postacrosomal part leading to a point where the FRAP approximation for circular bleach spots in an unbleached region of unlimited size and uniformity in all directions is highly questionable. This is illustrated in Fig. 7. Therefore we used CLSM to create a smaller bleach spot of 0.686 µm diameter with, due to the scanning nature of the laser beam, a bleaching time of about 300 ms. We detected rather low diffusion coefficients of about $0.5–3 \times 10^{-9}$ cm^2 s^{-1} which are in the typical range for membrane proteins being much larger in size and, therefore, diffuse slower. The diffusion coefficients calculated from our study by FCS for NBD analogs are around 60×10^{-9} cm^2 s^{-1} and are more consistent with expected motion characteristics of lipid molecules in a membrane (Stöckl et al. 2008). We are aware that due to the described aberrations of D when applying conventional FRAP analysis on confocal FRAP data, the D values revealed by FCS are more representative for the diffusional behavior of the applied lipid analogs.

Whereas no difference of NBD analog diffusion velocity between acrosomal and postacrosomal region was resolved by FCS, FRAP revealed significantly lower D values in the postacrosomal compared to the acrosomal part of the head for NBD-SM and NBD-PS. Lower D values in the postacrosomal compared to the acrosomal region were also found by FRAP for DiIC$_{12}$ in boar sperm (James et al. 2004) as well as for ODAF in bull, goat, monkey, mouse, and rat but not in boar, dog, and guinea pig sperm (Christova et al. 2004; Ladha et al. 1997; Wolfe et al. 1998). In the case of lower FRAP-derived D values in the postacrosome, these were concordantly interpreted by the authors in terms of a less fluid membrane in the posterior head.

Our FCS data matched quite well with the former examinations of ODAF in boar sperm membranes showing relatively homogenous diffusion coefficients over the whole sperm head in the dimension of 10^{-8} cm^2/s. While the different dimension of our FRAP-derived D values can be explained by the effect of bleach spot broadening as outlined above, this does not explain the inhomogeneity between both sperm head membrane regions seen with this technique. We hypothesize that our lower FRAP-derived D values of NBD-PS and NBD-SM in the postacrosome are not necessarily indicative of an overall slower diffusion or membrane fluidity in this part of the head but, on the

contrary, for the existence of subpopulations with heterogeneous diffusion coefficients. According to this hypothesis, the lower *D* values in the posterior region could be caused by a mixture of slowly as well as rapidly diffusing molecules. As a result of the mentioned effect of bleach spot broadening, the latter became unintentionally bleached to a higher extent. When analyzed by FCS, the same average *D* value as in the acrosomal region was detected without any information about the existence of putative lipid populations with different diffusion velocities. Compared to NBD-SM and NBD-PS, NBD-Ch does obviously not incorporate into different posterior membrane lipid populations with different diffusion behavior or can circumvent limitations in lateral diffusion by flip-flop. Mean *D* values as calculated from FRAP as well as FCS were similar in the acrosomal and postacrosomal region.

As concluded from comparing FRAP and FCS results (see above), the coexistence of subpopulations with different diffusion velocity is assumed for NBD-SM as well as NBD-PS in the postacrosomal region. The higher fluorescence lifetimes of NBD-PS and NBD-Ch in the acrosomal compared to the postacrosomal part (as possible consequence of decreased motional freedom in a suggested less fluid environment) would throughout be consistent with the assumption that rapidly and slowly diffusing label populations of NBD-SM and NBD-PS co-exist in the postacrosomal region. Fluorescence lifetimes of those differently diffusing analog subpopulations must not necessarily differ since the lifetime of NBD molecules in the order of several nanoseconds might rather be affected by immediate molecular surroundings. The fluorescence lifetimes can be similar in a continuous lipid phase as well as within molecular platforms/domains which, as a whole, show restricted diffusion in a much larger spatial and temporal scale as detected with FRAP and FCS.

Conclusions

In conclusion, we could show that a combination of different microscopic methods provides a comprehensive picture of lipid dynamics in the cell membrane of vital sperm even if conclusions from each single method are limited and fragmentary in the respective temporal and spatial window. The presented lipid-analog-specific results indicate that the lipid analogs used are suitable to report on the conditions of surrounding membrane domains with different properties. Whereas FLIM analyses did not indicate coexisting distinct liquid-ordered and -disordered domains in any of the head regions, particularly FRAP in comparison to FCS measurements suggest the incorporation of NBD-SM as well as NBD-PS in postacrosomal subpopulations with different diffusion velocity. FLIM analyses further indicate a more fluid microenvironment of NBD-Ch and NBD-PS in the postacrosomal compared to the acrosomal region indicating a more fluid cytoplasmic leaflet compared to the exoplasmic one. This conclusion is supported by lower fluorescence lifetime and higher *D* values (FCS) for NBD-PS in both head compartments.

For the first time, fluorescence lifetimes of lipid analogs were determined in the sperm cell membrane and found to be in a range characteristic for the liquid-disordered phase in artificial lipid membranes (GUV). Sperm require a fragile membrane with fusion competence for acrosome reaction and fertilization which for instance becomes apparent in the high amount of polyunsaturated fatty acyl residues in sperm lipids. Moreover, boar sperm contain less cholesterol, e.g., compared to bull sperm (Parks and Lynch 1992), a lipid which rigidifies membranes. The binding of components, e.g., seminal plasma proteins to sperm, could modify their physico-chemical membrane properties. As we have shown recently, bull sperm membranes are stabilized—a requirement for the transit through the female genital tract—by seminal fluid proteins, which directly interact with the lipid phase (Greube et al. 2001; Tannert et al. 2007b). It remains to be investigated whether boar seminal proteins are also able to affect membrane properties, e.g., to stabilize the comparatively fluid sperm membrane.

Acknowledgments This work was supported by the German Research Council (DFG MU1520/2-1) and by the German Ministry of Education and Research (BMBF Number 033 L046). The authors thank Andreas Herrmann and Thomas Korte (Humboldt-University Berlin) for helpful advice and discussion. The authors also appreciate the excellent technical assistance of Anita Retzlaff (Institute for Reproduction of Farm Animals Schönow e.V.) and Jenny Eichhorst (Leibniz Institute for Molecular Pharmacology).

References

Adkins EM, Samuvel DJ, Fog JU, Eriksen J, Jayanthi LD, Vaegter CB, Ramamoorthy S, Gether U (2007) Membrane mobility and microdomain association of the dopamine transporter studied with fluorescence correlation spectroscopy and fluorescence recovery after photobleaching. Biochemistry 46:10484–10497

Almeida PF, Pokorny A, Hinderliter A (2005) Thermodynamics of membrane domains. Biochim Biophys Acta 1720:1–13

Amaro M, Sachl R, Jurkiewicz P, Coutinho A, Prieto M, Hof M (2014) Time-resolved fluorescence in lipid bilayers: selected applications and advantages over steady state. Biophys J 107:2751–2760

Axelrod D, Koppel DE, Schlessinger J, Elson E, Webb WW (1976) Mobility measurement by analysis of fluorescence photobleaching recovery kinetics. Biophys J 16:1055–1069

Boerke A, Tsai PS, Garcia-Gil N, Brewis IA, Gadella BM (2008) Capacitation-dependent reorganization of microdomains in the apical sperm head plasma membrane: functional relationship with zona binding and the zona-induced acrosome reaction. Theriogenology 70:1188–1196

Bou Khalil M, Chakrabandhu K, Xu H, Weerachatyanukul W, Buhr M, Berger T, Carmona E, Vuong N, Kumarathasan P, Wong PT, Carrier D, Tanphaichitr N (2006) Sperm capacitation induces an increase in lipid rafts having zona pellucida binding ability and containing sulfogalactosylglycerolipid. Dev Biol 290:220–235

Braga J, Desterro JM, Carmo-Fonseca M (2004) Intracellular macromolecular mobility measured by fluorescence recovery after photobleaching with confocal laser scanning microscopes. Mol Biol Cell 15:4749–4760

Chattopadhyay A (1990) Chemistry and biology of *N*-(7-nitrobenz-2-oxa-1,3-diazol-4-yl)-labeled lipids: fluorescent probes of biological and model membranes. Chem Phys Lipid 53:1–15

Christova Y, James P, Mackie A, Cooper TG, Jones R (2004) Molecular diffusion in sperm plasma membranes during epididymal maturation. Mol Cell Endocrinol 216:41–46

Daleke DL (2003) Regulation of transbilayer plasma membrane phospholipid asymmetry. J Lipid Res 44:233–242

de Almeida RF, Loura LM, Prieto M (2009) Membrane lipid domains and rafts: current applications of fluorescence lifetime spectroscopy and imaging. Chem Phys Lipids 157:61–77

Eckford PD, Sharom FJ (2005) The reconstituted P-glycoprotein multidrug transporter is a flippase for glucosylceramide and other simple glycosphingolipids. Biochem J 389:517–526

Elson EL (2001) Fluorescence correlation spectroscopy measures molecular transport in cells. Traffic 2:789–796

Fery-Forgues S, Fayet JP, Lopez A (2003) Drastic changes in the fluorescence properties of NBD probes with the polarity of the medium: involvement of a TICT state? J Photochem Photobiol A Chem 70:229–243

Fuchs B, Jakop U, Goritz F, Hermes R, Hildebrandt T, Schiller J, Müller K (2009) MALDI-TOF "fingerprint" phospholipid mass spectra allow the differentiation between Ruminantia and Feloideae spermatozoa. Theriogenology 71:568–575

Gadella BM, Miller NG, Colenbrander B, van Golde LM, Harrison RA (1999) Flow cytometric detection of transbilayer movement of fluorescent phospholipid analogues across the boar sperm plasma membrane: elimination of labeling artifacts. Mol Reprod Dev 53:108–125

Greube A, Müller K, Töpfer-Petersen E, Herrmann A, Müller P (2001) Influence of the bovine seminal plasma protein PDC-109 on the physical state of membranes. Biochemistry 40:8326–8334

Guo L, Har JY, Sankaran J, Hong Y, Kannan B, Wohland T (2008) Molecular diffusion measurement in lipid bilayers over wide concentration ranges: a comparative study. ChemPhysChem 9:721–728

Haldar S, Chattopadhyay A (2013) Application of NBD-labeled lipids in membrane and cell biology. In: Mely Y, Duportail G (eds) Fluorescent methods to study biological membranes. Springer, Berlin, pp 37–50

Haupts U, Maiti S, Schwille P, Webb WW (1998) Dynamics of fluorescence fluctuations in green fluorescent protein observed by fluorescence correlation spectroscopy. Proc Natl Acad Sci USA 95:13573–13578

Howes EA, Hurst SM, Jones R (2001) Actin and actin-binding proteins in bovine spermatozoa: potential role in membrane remodeling and intracellular signaling during epididymal maturation and the acrosome reaction. J Androl 22:62–72

Ikawa M, Inoue N, Benham AM, Okabe M (2010) Fertilization: a sperm's journey to and interaction with the oocyte. J Clin Invest 120:984–994

Im JS, Yu KO, Illarionov PA, LeClair KP, Storey JR, Kennedy MW, Besra GS, Porcelli SA (2004) Direct measurement of antigen binding properties of CD1 proteins using fluorescent lipid probes. J Biol Chem 279:299–310

James PS, Wolfe CA, Ladha S, Jones R (1999) Lipid diffusion in the plasma membrane of ram and boar spermatozoa during maturation in the epididymis measured by fluorescence recovery after photobleaching. Mol Reprod Dev 52:207–215

James PS, Hennessy C, Berge T, Jones R (2004) Compartmentalisation of the sperm plasma membrane: a FRAP, FLIP and SPFI analysis of putative diffusion barriers on the sperm head. J Cell Sci 117:6485–6495

Jamil K (1984) Plasma membrane cytoskeletal complex of the mammalian spermatozoa. Arch Androl 13:177–193

Jones R, James PS, Howes L, Bruckbauer A, Klenerman D (2007) Supramolecular organization of the sperm plasma membrane during maturation and capacitation. Asian J Androl 9:438–444

Jones R, Howes E, Dunne PD, James P, Bruckbauer A, Klenerman D (2010) Tracking diffusion of GM1 gangliosides and zona pellucida binding molecules in sperm plasma membranes following cholesterol efflux. Dev Biol 339:398–406

Julien M, Tournier JF, Tocanne JF (1993) Differences in the transbilayer and lateral motions of fluorescent analogs of phosphatidylcholine and phosphatidylethanolamine in the apical plasma membrane of bovine aortic endothelial cells. Exp Cell Res 208:387–397

Kang M, Day CA, Drake K, Kenworthy AK, DiBenedetto E (2009) A generalization of theory for two-dimensional fluorescence recovery after photobleaching applicable to confocal laser scanning microscopes. Biophys J 97:1501–1511

Kang M, Day CA, Kenworthy AK, DiBenedetto E (2012) Simplified equation to extract diffusion coefficients from confocal FRAP data. Traffic 13:1589–1600

Kawano N, Yoshida K, Miyado K, Yoshida M (2011) Lipid rafts: keys to sperm maturation, fertilization, and early embryogenesis. J Lipid 2011:264706

Klein AS, Schaefer M, Korte T, Herrmann A, Tannert A (2012) HaCaT keratinocytes exhibit a cholesterol and plasma membrane viscosity gradient during directed migration. Exp Cell Res 318:809–818

Kol MA, van Dalen A, de Kroon AI, de Kruijff B (2003) Translocation of phospholipids is facilitated by a subset of membrane-spanning proteins of the bacterial cytoplasmic membrane. J Biol Chem 278:24586–24593

Kurz A, Viertel D, Herrmann A, Müller K (2005) Localization of phosphatidylserine in boar sperm cell membranes during capacitation and acrosome reaction. Reproduction 130:615–626

Ladha S, James PS, Clark DC, Howes EA, Jones R (1997) Lateral mobility of plasma membrane lipids in bull spermatozoa: heterogeneity between surface domains and rigidification following cell death. J Cell Sci 110(Pt 9):1041–1050

Lessig J, Gey C, Suss R, Schiller J, Glander HJ, Arnhold J (2004) Analysis of the lipid composition of human and boar spermatozoa by MALDI-TOF mass spectrometry, thin-layer chromatography and 31P NMR spectroscopy. Comp Biochem Physiol B Biochem Mol Biol 137:265–277

Lin S, Struve WS (1991) Time-resolved fluorescence of nitrobenzoxadiazole-aminohexanoic acid: effect of intermolecular hydrogen-bonding on non-radiative decay. Photochem Photobiol 54:361–365

Luconi M, Barni T, Vannelli GB, Krausz C, Marra F, Benedetti PA, Evangelista V, Francavilla S, Properzi G, Forti G, Baldi E (1998) Extracellular signal-regulated kinases modulate capacitation of human spermatozoa. Biol Reprod 58:1476–1489

Mackie AR, James PS, Ladha S, Jones R (2001) Diffusion barriers in ram and boar sperm plasma membranes: directionality of lipid diffusion across the posterior ring. Biol Reprod 64:113–119

Mukherjee S, Maxfield FR (2004) Membrane domains. Annu Rev Cell Dev Biol 20:839–866

Mukherjee S, Kalipatnapu S, Pucadyil TJ, Chattopadhyay A (2006) Monitoring the organization and dynamics of bovine hippocampal membranes utilizing differentially localized fluorescent membrane probes. Mol Membr Biol 23:430–441

Müller K, Pomorski T, Müller P, Zachowski A, Herrmann A (1994) Protein-dependent translocation of aminophospholipids and asymmetric transbilayer distribution of phospholipids in the plasma membrane of ram sperm cells. Biochemistry 33:9968–9974

Müller P, Plazzo AP, Herrmann A (2011) Transbilayer movement and distribution of cholesterol. In: Devaux PF (ed) Membrane asymmetry and transmembrane motion of lipids. Wiley, Hoboken, pp 75–96

Nolan JP, Magargee SF, Posner RG, Hammerstedt RH (1995) Flow cytometric analysis of transmembrane phospholipid movement in bull sperm. Biochemistry 34:3907–3915

Ostasov P, Sykora J, Brejchova J, Olzynska A, Hof M, Svoboda P (2013) FLIM studies of 22- and 25-NBD-cholesterol in living HEK293 cells: plasma membrane change induced by cholesterol depletion. Chem Phys Lipid 167–168:62–69

Parks JE, Lynch DV (1992) Lipid composition and thermotropic phase behavior of boar, bull, stallion, and rooster sperm membranes. Cryobiology 29:255–266

Peterson RN, Gillott M, Hunt W, Russell LD (1987) Organization of the boar spermatozoan plasma membrane: evidence for separate domains (subdomains) of integral membrane proteins in the plasma membrane overlying the principal segment of the acrosome. J Cell Sci 88(Pt 3):343–349

Pomorski T, Herrmann A, Zachowski A, Devaux PF, Müller P (1994) Rapid determination of the transbilayer distribution of NBD-phospholipids in erythrocyte membranes with dithionite. Mol Membr Biol 11:39–44

Pomorski T, Hrafnsdottir S, Devaux PF, van Meer G (2001) Lipid distribution and transport across cellular membranes. Semin Cell Dev Biol 12:139–148

Pucadyil TJ, Mukherjee S, Chattopadhyay A (2007) Organization and dynamics of NBD-labeled lipids in membranes analyzed by fluorescence recovery after photobleaching. J Phys Chem B 111:1975–1983

Ramstedt B, Slotte JP (2006) Sphingolipids and the formation of sterol-enriched ordered membrane domains. Biochim Biophys Acta 1758:1945–1956

Seigneuret M, Zachowski A, Hermann A, Devaux PF (1984) Asymmetric lipid fluidity in human erythrocyte membrane: new spin-label evidence. Biochemistry 23:4271–4275

Sengupta P, Hammond A, Holowka D, Baird B (2008) Structural determinants for partitioning of lipids and proteins between coexisting fluid phases in giant plasma membrane vesicles. Biochim Biophys Acta 1778:20–32

Sezgin E, Levental I, Grzybek M, Schwarzmann G, Mueller V, Honigmann A, Belov VN, Eggeling C, Coskun U, Simons K, Schwille P (2012) Partitioning, diffusion, and ligand binding of raft lipid analogs in model and cellular plasma membranes. Biochim Biophys Acta 1818:1777–1784

Simons K, Gerl MJ (2010) Revitalizing membrane rafts: new tools and insights. Nat Rev Mol Cell Biol 11:688–699

Stöckl M, Plazzo AP, Korte T, Herrmann A (2008) Detection of lipid domains in model and cell membranes by fluorescence lifetime imaging microscopy of fluorescent lipid analogues. J Biol Chem 283:30828–30837

Tannert A, Kurz A, Erlemann KR, Müller K, Herrmann A, Schiller J, Töpfer-Petersen E, Manjunath P, Müller P (2007a) The bovine seminal plasma protein PDC-109 extracts phosphorylcholine-containing lipids from the outer membrane leaflet. Eur Biophysi J EBJ 36:461–475

Tannert A, Töpfer-Petersen E, Herrmann A, Müller K, Müller P (2007b) The lipid composition modulates the influence of the bovine seminal plasma protein PDC-109 on membrane stability. Biochemistry 46:11621–11629

Tanphaichitr N, Carmona E, Bou Khalil M, Xu H, Berger T, Gerton GL (2007) New insights into sperm-zona pellucida interaction: involvement of sperm lipid rafts. Front Biosci 12:1748–1766

Teichmann A, Gibert A, Lampe A, Grzesik P, Rutz C, Furkert J, Schmoranzer J, Krause G, Wiesner B, Schulein R (2014) The specific monomer/dimer equilibrium of the corticotropin-releasing factor receptor type 1 is established in the endoplasmic reticulum. J Biol Chem 289:24250–24262

van Gestel RA, Brewis IA, Ashton PR, Helms JB, Brouwers JF, Gadella BM (2005) Capacitation-dependent concentration of lipid rafts in the apical ridge head area of porcine sperm cells. Mol Hum Reprod 11:583–590

Wang TY, Silvius JR (2000) Different sphingolipids show differential partitioning into sphingolipid/cholesterol-rich domains in lipid bilayers. Biophys J 79:1478–1489

Wang TY, Silvius JR (2003) Sphingolipid partitioning into ordered domains in cholesterol-free and cholesterol-containing lipid bilayers. Biophys J 84:367–378

Wolfe CA, James PS, Mackie AR, Ladha S, Jones R (1998) Regionalized lipid diffusion in the plasma membrane of mammalian spermatozoa. Biol Reprod 59:1506–1514

Wustner D (2007) Fluorescent sterols as tools in membrane biophysics and cell biology. Chem Phys Lipid 146:1–25

Wustner D, Pomorski T, Herrmann A, Müller P (1998) Release of phospholipids from erythrocyte membranes by taurocholate is determined by their transbilayer orientation and hydrophobic backbone. Biochemistry 37:17093–17103

Wustner D, Mukherjee S, Maxfield FR, Müller P, Herrmann A (2001) Vesicular and nonvesicular transport of phosphatidylcholine in polarized HepG2 cells. Traffic 2:277–296

Zachowski A (1993) Phospholipids in animal eukaryotic membranes: transverse asymmetry and movement. Biochem J 294(Pt 1):1–14